ResearchGate

See discussions, stats, and author profiles for this publication at: https://www.researchgate.net/publication/268529343

Effect of surface coating on the biocompatibility and in vivo MRI detection of iron oxide nanoparticles after intrapulmonary administration

Article *in* Nanotoxicology · November 2014

DOI: 10.3109/17435390.2014.980450

CITATIONS
15

READS
242

3 authors, including:

Achraf Al Faraj
American University of Science and Technology
43 PUBLICATIONS **519** CITATIONS

SEE PROFILE

Some of the authors of this publication are also working on these related projects:

Nanoparticles for health View project

Pharmacometabolomics View project

All content following this page was uploaded by Achraf Al Faraj on 05 January 2015.

The user has requested enhancement of the downloaded file.

http://informahealthcare.com/nan
ISSN: 1743-5390 (print), 1743-5404 (electronic)

Nanotoxicology

Nanotoxicology, Early Online: 1–10
© 2014 Informa UK Ltd. DOI: 10.3109/17435390.2014.980450

informa
healthcare

ORIGINAL ARTICLE

Effect of surface coating on the biocompatibility and *in vivo* MRI detection of iron oxide nanoparticles after intrapulmonary administration

Achraf Al Faraj[1]*, Abjal Pasha Shaik[2]*, and Asma Sultana Shaik[1,3]

[1]*College of Applied Medical Sciences, King Saud University, Riyadh, Saudi Arabia,* [2]*Department of Clinical Lab Sciences, College of Applied Medical Sciences, King Saud University, Riyadh, Saudi Arabia, and* [3]*Prince Naif Center for Immunology Research, College of Medicine, King Saud University, Riyadh, Saudi Arabia*

Nanotoxicology Downloaded from informahealthcare.com by 212.215.215.114 on 11/19/14
For personal use only.

Abstract

Superparamagnetic iron oxide nanoparticles (SPIONs) have attracted special attention as novel nanoprobes capable of improving both the therapy and diagnosis of lung diseases. For safe prospective clinical applications, their biocompatibility has to be assessed after intrapulmonary administration. This study was therefore conducted to understand the biological impact of SPIONs and their further surface-functionalization with polyethylene glycol (PEG) having either negative (i.e. carboxyl) or positive (i.e. amine) terminal in a 1-month longitudinal study following acute and sub-acute exposures. Noninvasive free-breathing MR imaging protocols were first optimized to validate SPIONs detection in the lung and investigate possible subsequent systemic translocation to abdominal organs. Pulmonary Magnetic Resonance Imaging (MRI) allowed successful *in vivo* detection of SPIONs in the lung using ultra-short echo time sequence. Following high-dose lung administration, MR imaging performed on abdominal organs detected transient accumulation of SPIONs in the liver. Iron quantification using Inductive coupled plasma – Mass mass spectroscopy (ICP-MS) confirmed MRI readouts. Oxidative stress induction and genotoxicity were then conducted to evaluate the biocompatibility of SPIONs with their different formulations in a mouse model. A significant increase in lipid peroxidation was observed in both acute and sub-acute sets and found to regress in a time-dependent manner. PEG functionalized SPIONs revealed a lower effect with no difference between both terminal modifications. Genotoxicity assessments revealed an increase in DNA damage and gene expression of CCL-17 and IL-10 biomarkers following SPIONs administration, which was significantly higher than surface-modified nanoparticles and decreased in a time-dependent manner. However, SPIONs with carboxyl terminal showed a slightly prominent effect compared to amine modification.

Keywords

Lung imaging, MRI, nanotoxicity, superparamagnetic iron oxide nanoparticles, surface charge coating

History

Received 12 June 2014
Revised 8 October 2014
Accepted 16 October 2014
Published online 19 November 2014

Introduction

Pulmonary delivery of drug-loaded nanocarriers has emerged as a promising alternative for the treatment and prevention of lung diseases (Azarmi et al., 2008; Sung et al., 2007; van Rijt et al., 2014). With its high surface area, thin epithelial barriers and extensive vasculature, the lung represents an excellent entry portal for inhaled nanoparticles, which may then have the ability to get deposited with high efficiency throughout the entire respiratory system and pulmonary tissues (Geiser & Kreyling, 2010). Lung physiology allows for noninvasive drug delivery, especially for low water-soluble therapeutics that have poor bioavailability via oral administration (Bailey & Berkland, 2009). This targeted delivery can therefore potentially reduce the overall dose, and thus any side effects that result from high levels of systemic administration. It also offers direct action by avoiding the first-pass metabolism for delivery of biotherapeutics (i.e. peptides and proteins) that cannot be delivered orally owing to enzymatic degradation and poor intestinal membrane permeability (Hamman et al., 2005). Moreover, specific lung cells such as alveolar macrophages can be specifically targeted for the treatment of diseases such as asthma, COPD or tuberculosis (Al Faraj et al., 2014a; Chellat et al., 2005).

From the different available nanoparticle formulations, superparamagnetic iron oxide nanoparticles (SPIONs) have attracted huge scientific attention for such applications due to their superior biocompatibility, ability to cross biological membranes, appropriate surface architecture and easy conjugation with targeting ligands (Xu & Sun, 2013). In the last decade, biomedical interest of SPIONs has significantly increased due to their use in magnetic separation techniques, as contrast agents in Magnetic Resonance Imaging (MRI), hyperthermia, tissue repair and/or as magnetic-targeted nanocarriers for drug delivery systems (DDS) (Rosen et al., 2012; Wahajuddin & Arora, 2012). Recent advances in the design of engineered SPIONs have offered new perspectives for novel theranostics capable of improving both the therapy and

*Both authors contributed equally to this work.

Correspondence: Achraf Al Faraj, College of Applied Medical Sciences, King Saud University, Riyadh 11433, Saudi Arabia. Tel: +966 11 46 96017/99664. Fax: +966 11 46 93565. E-mail: aalfaraj@ksu.edu.sa

RIGHTSLINK

diagnosis of pulmonary diseases in a single multifunctional platform (Yoo et al., 2011).

From a toxicological point of view, the different physico-chemical properties of nanoparticles such as their size, shape, surface charge, chemical properties, solubility and degree of agglomeration determine their effects on biological systems and human health (Braakhuis et al., 2014), and thus, the likelihood for their applications as DDS. Numerous preclinical and clinical studies have been conducted using SPIONs, resulting in their clinical approval for intravenous and oral administration (Bernd et al., 2009; Corot et al., 2006). Similarly, for prospective clinical pulmonary applications of SPIONs-based nanocarriers as theranostic tools for lung diseases, their biocompatibility should be carefully assessed under *in vitro* and *in vivo* longitudinal follow-up protocols.

Most studies conducted to assess the role of surface charge in cellular uptake and cytotoxicity of medical nanoparticles were mainly performed *in vitro* (Frohlich, 2012). However, the effects of SPION surface charge after their *in vivo* pulmonary administration is still not conclusive. In addition, the *in vivo* effect of pulmonary administration of SPIONs and their surface functionalization on genotoxicity (i.e. DNA damage) and ability to cause oxidative stress need to be demonstrated as a part of *in vivo* biocompatibility testing (Mbeh et al., 2012; Singh et al., 2012).

The purpose of this study was thus to assess the genotoxicity and oxidative stress induced following either acute or sub-acute intrapulmonary administration of dextran-coated SPIONs in a 1-month longitudinal follow-up study, while validating their noninvasive detection in the lung using MRI and their possible subsequent translocation and deposition in systemic sites such as liver, spleen, kidneys and blood. The effect of SPIONs functionalization with polyethylene glycol with either negative (i.e. carboxyl) or positive (i.e. amine) terminals was investigated.

Nanotoxicology Downloaded from informahealthcare.com by 212.215.215.114 on 11/19/14
For personal use only.

Materials and methods

SPIONs preparation and characterization

Nanoferrite superparamagnetic iron oxide nanoparticles prepared via the core–shell method with a core of 75–80% (w/w) magnetite and a shell of dextran (Micromod Partikeltechnologie GmbH, Rostock, Germany) were used in this study (Grüttner et al., 2007). They were then cross-linked with a mixture of polyethylene glycol diglycidyl ether (MW = 526), and epichlorohydrin at pH 11−12 for 24 h at room temperature and suspended in deionized water after magnetic separation. For amine modification, SPIONs were functionalized with amino groups by shaking with ammonia for 24 h at room temperature. NH_2-functionalized iron oxide nanoparticles were washed with deionized water and filtered through 0.22 µm Millex-GP filters (Millipore, Billerica, MA). For carboxyl modification, SPIONs were further modified by EDC (1-ethyl-3-(3-dimethylaminopropyl)-carbodiimide HCl) and PEG 600 diacid using MES (2-(4-morpholino)ethanesulphonic acid) buffer (pH 6.3) purchased from Sigma Aldrich (St. Louis, MO) and incubated for 2 h at room temperature.

Size and zeta potential

The size and zeta potential (i.e. electrical surface charge) of SPIONs before and after their surface modification were first determined using a Zetasizer Nano ZS90 (Malvern Instruments, Malvern, UK) as previously described (Al Faraj et al., 2014b). These nanoparticles were analyzed at a concentration range of 0.01–1 mg/ml in homogenously dispersed ultrapure water suspension at pH 7.

Transmission electron microscopy

Transmission Electron Microscopy (TEM) was then used to obtain characteristic images of each SPIONs and check the size and shape of the nanoparticles. Images were obtained using an EM 912 (Zeiss, Oberkochen, Germany) operating at 100 keV. Nanoparticle solutions were diluted and allowed to dry on a carbon film.

MR relaxivities

Longitudinal ($r1$) and transverse ($r2^*$) relaxivities of SPIONs were then measured at 25 °C on tubes containing suspension of nanoparticles at different iron concentrations (0, 0.10, 0.15, 0.20, 0.40, 0.60, 0.80 mM) using a 4.7T Pharmascan 47/16 Bruker magnet interfaced to ParaVision 5.1 software (Bruker Biospin GmbH, Rheinstetten, Germany). For the measurement of T1 relaxation time, an inversion-recovery fast imaging with steady state precession (IR-FISP) sequence was used with TR/TE = 4/2 ms, and an increasing inversion time starting from $T1 = 100$ ms with 60 echoes. For the measurement of $T2^*$ relaxation time, a Multi Gradient Echo (MGE) sequence was used with a TR of 1500 ms and increasing TEs starting from 4 ms with 15 echoes of 4 ms echo spacing. $T1$ and $T2^*$ relaxation times were automatically calculated using the Paravision image analysis software. Relaxivities were then calculated as the slope of the linear regression generated from a plot of the measured relaxation rate ($1/Ti$, where $i = 1$ or 2^*) versus the concentration of the particles. $(1/Ti) = (1/Ti(0)) + ri[\text{SPIO}]$ where Ti denotes the relaxation times of a suspension containing the particles and $Ti(0)$ is the relaxation time of the solvent (water) without particles.

Experimental protocol

Balb/c mice (16–18 g) used in this study were obtained from the University's main animal care center. All experiments were performed in accordance with the National guidelines for the care of laboratory animals after approval by the Ethical Committee of the College of Applied Medical Sciences (agreement number: CAMS07/3334). During the different imaging protocols, each animal was anesthetized by intramuscular administration of a mixture of 0.1 mL of 4 mL of ketamine (500 mg/mL), 1 mL of xylazine (2%) and 5 mL of physiological serum. Animals were divided into two treatment groups for assessing the effect of SPIONs acute (i.e. single-dose intrapulmonary administration) or sub-acute (i.e. three consecutive doses with 24 h intervals) toxicity. In each set, mice were divided in four groups ($n = 3$ per group): ''Control'' mice received an intrapulmonary administration of physiological saline solution [$V = 100$ µL]), whereas ''SPION'', ''SPION + PEG-COOH'' and ''SPION + PEG-NH_2'' mice received per dose an intrapulmonary administration of SPIONs with iron concentration of 2 mM corresponding to 0.8 mmol of iron kg^{-1} in 100 µL water suspension. Lung administration was performed using a MicroSprayer aerosolizer – Model IA-1C (Penn-Century Inc., Wyndmoor, PA) which has been shown to allow homogenous distribution of administered materials in the lung (Al Faraj et al., 2014a).

Magnetic resonance imaging

For both pulmonary and abdominal imaging, mice were imaged at 2 h, 24 h, 48 h and 1 week in acute treatment groups, or underwent MR imaging protocols at 24 h, 1 week, 2 weeks and 1 month after the last SPIONs exposition in sub-acute treatment groups.

Pulmonary imaging

To validate SPION detection in the lung, noninvasive free-breathing pulmonary MR imaging was performed on the 4.7 T

RIGHTSLINK

Nanotoxicology Downloaded from informahealthcare.com by 212.215.215.114 on 11/19/14
For personal use only.

Bruker magnet using a radial ultra-short time of echo (UTE) sequence with the following parameters: TR/TE = 100/0.4 ms, in plane resolution = 100 × 100 μm, flip angle = 15°, 4 averages. Axial slices with 1 mm thickness ($n = 10$) were positioned to cover the entire lung volume.

Systemic abdominal imaging

To assess the possibility of SPIONs translocation to systemic abdominal organs after intrapulmonary administration following the different treatments, axial slices with 1 mm thickness ($n = 20$) were positioned over organs of interest such as the liver, spleen and kidneys. MR imaging was performed using a susceptibility-weighted gradient echo sequence with the following parameters: TR/TE = 300/3 ms, in plane pixel resolution = 100 × 100 μm, flip angle = 30°, 4 averages.

An ultrapure water tube was positioned over the body of the mice as external reference to normalize the MR signal and allow measurement of contrast-to-noise ratio (CNR) variation in the different regions of interests as previously described (Al Faraj et al., 2014b).

Following MR imaging protocols, mice were sacrificed by lethal overdose injection of anesthesia at 2 h, 24 h and 1 week following SPIONs administration in acute treatment groups and at 24 h, 1 week and 1 month in sub-acute treatment groups. Broncho-alveolar lavage fluid (BALF), lung, liver, spleen and kidneys were then removed for the different post-mortem analysis as described below.

Inductive coupled plasma – mass spectroscopy (ICP-MS)

Quantification of iron following intrapulmonary administration of SPIONs with different surface charge in both acute and sub-acute sets was performed on lung, liver, spleen and kidneys using ICPMS as per the Standard Operation Procedure for Analysis of Major, Minor and Trace Elements in Animal Tissue Samples. Tissue samples were digested with ultrapure 69% nitric acid (HNO_3) (Panreac, Barcelona, Spain) and processed in Mars 6 microwave digestion system (MARS 6, CEM, Mars Hill, NC). Iron concentrations were then quantified using an Aurora M90 ICP-MS system (Bruker, Billerica, MA) and reported as mg Fe/g sample.

Oxidative stress evaluation (TBARS assay)

BALF and lung biopsy samples were collected from mice at the different investigation time points to evaluate the relative lipid peroxidation content as index of overall oxidative stress induced by the different SPIONs formulations in both acute and sub-acute animal sets using Thiobarbituric Acid Reactive Substances (TBARS) Parameter Assay Kit (R&D systems, Minneapolis, MN) as per the manufacturer's protocol. Cells obtained from BALF and lung tissues were washed and lysed with cell lysis buffer for 30 min followed by incubation with acid reagent for 15 min. The supernatants obtained after centrifugation were treated with TBA reagent and incubated for a further 2–3 h at 45–50 °C and optical density of the samples was measured at 532 nm using Multiskan Go Microplate Spectrophotometer (Thermo Scientific, Hudson, NH).

DNA damage assessment (comet assay)

Comet assay, also known as single-cell gel electrophoresis assay, was used as an effective method to assess the possible DNA damage induced by the iron oxide nanoparticles. Cells from BALF and lung biopsy samples were prepared for comet assay as per the specified protocol (R&D systems, Minneapolis, MN). Cells were immobilized in low-melting agarose, lysed after denaturation of DNA in alkali buffer, electrophoresed at pH > 13 and silver stained. The cells were then observed under an Olympus BX53 microscope (Olympus Corporation, Tokyo, Japan). Data for DNA damage are presented as mean ± SD for an average of 100 cells.

Gene expression profile (real-time polymerase chain reaction)

To evaluate the relative gene expression profiles in selected cytokines, RNA was first isolated from BALF and lung tissue samples using TRIzol® LS reagent (Life Technologies, Carlsbad, CA). Reverse transcription of RNA to cDNA was performed using RNA M-MLV reverse transcriptase (Promega Corporation, Maddison, WI). Amplification of cDNA was then performed by real-time quantitative SYBR green chemistry PCR using an ABI Prism 7700 (Applied Biosystems, Foster City, CA) sequence detection system. Glyceraldehyde 3-phosphate dehydrogenase (GAPDH) was analyzed as an internal control. Relative gene expression of NOS-2, CXCL-10, CCL-17, CCL-22 and IL-10 genes was evaluated using specific primers from Integrated DNA Technologies (Leuven, Belgium, China). Primers for NOS-2 were 5′-CGCAGCTGGGCTGTACCAA-3′ and 5′-TGATGTTTGCTTCGGACATCA-3′; for CXCL-10, 5′-GCTGCCGTCATTTTCTGC-3′ and 5′-TCTCACTGGCCCGTCATC-3′; for CCL-17, 5′-TGCTTCTGGGGACTTTTCTG-3′ and 5′-GAATGGCCCCTTTGAGTAA-3′; for CCL-22, 5′-TCTTGCTGTGGCAATTCAGA-3′ and 5′-GAGGGTGACGGATGTAGTCC-3′ and for IL-10, 5′-GAAGCATGGCCCAGAAATCA-3′ and 5′-TGCTCCACTGCCTTGCTCTT-3′. Gene expression in all treated mice was presented as a fold increase relative to the control mice. The fold difference in gene expression profiles between the different groups was determined using Applied Biosystems analysis manager (Foster City, CA).

Statistical analysis

Data presented as the mean standard deviation were analyzed by the *t*-test using SPSS version 12.0 (SPSS Inc., Chicago, IL) software. p values <0.05 were considered significant for all tests.

Results

SPIONs characterization

SPIONs functionalization with polyethylene glycol having either negative (i.e. PEG-COOH) or positive (i.e. PEG-NH_2) terminals showed a slight increase in the mean size of the nanoparticles with an average size of 129.3 ± 8.3 nm for SPIONs. The size of SPIONs agglomerates was rechecked after collecting the suspensions aerosolized using the Microsprayer device (i.e. droplets containing nanosized SPIONs) and similar values were obtained (Supplementary data). Zeta potential analysis confirmed a negatively charged particle with −3.48 ± 0.32 mV after PEG-COOH conjugation and a positively charged particle with 2.87 ± 0.44 mV after PEG-NH_2 surface modification (Table 1). The shape and size of SPIONs were confirmed using TEM images (Figure 1), which showed no difference among the different nanoparticle formulations. Measurements of $r2^*$ relaxivities performed at 4.7 T revealed a high $r2^*$ values (i.e. 253.92 ± 7.53 $mM^{-1} s^{-1}$ for SPIONs) for all formulations with no statistically significant variations after surface modification. For all samples, $r1$ values were found negligible (0.06 ± 0.01 $mM^{-1} s^{-1}$).

Following SPIONs intrapulmonary administration using the MicroSprayer aerosolizer, all mice survived following both acute and sub-acute exposures, and did not show any sign of discomfort (i.e. lethargy, nausea, vomiting or diarrhea) during the whole duration of the follow-up investigations.

RIGHTSLINK

Table 1. Superparamagnetic iron oxide nanoparticles mean size, zeta potential and $r1$ and $r2^*$ relaxivities before and after either PEG-COOH or PEG-NH2 surface functionalization.

	Mean size (nm)	Zeta potential (mV)	$r1$ relaxivity ($mM^{-1}\,s^{-1}$)	$r2^*$ relaxivity ($mM^{-1}\,s^{-1}$)
SPION	129.3 ± 8.3	0.71 ± 0.28	0.06 ± 0.01	253.92 ± 7.53
SPION + PEG-COOH	135.6 ± 7.2	-3.48 ± 0.32	0.06 ± 0.01	245.22 ± 6.72
SPION + PEG-NH_2	133.2 ± 6.6	2.87 ± 0.44	0.06 ± 0.01	241.89 ± 8.43

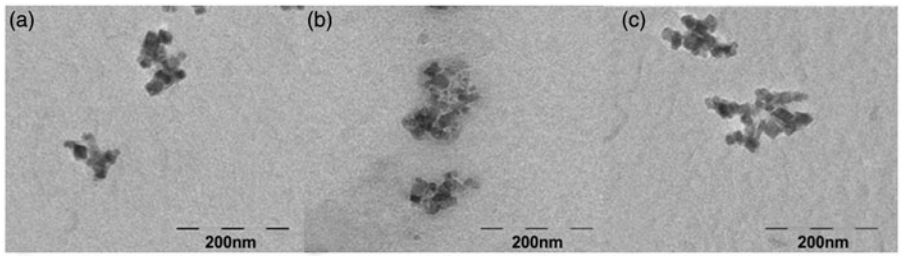

Figure 1. Representative Transmission Electron Microscopy (TEM) images of SPIONs before (a) and after either PEG-COOH (b) or PEG-NH_2 (c) surface functionalization.

Nanotoxicology Downloaded from informahealthcare.com by 212.215.215.114 on 11/19/14
For personal use only.

Magnetic resonance imaging

Pulmonary MR imaging, performed under a free-breathing protocol using UTE sequence, detected of an overall MR signal attenuation related to the presence of SPIONs in the lung with the maximum effect observed at 2 h post-administration in acute treatment groups and 24 h post-administration in sub-acute treatment groups (Figure 2). No difference in CNR attenuation was observed following lung exposure with the different SPION formulations (i.e. positively or negatively charged iron oxide nanoparticles). Quantitatively, following SPION administration in the acute treatment group, CNR value of $71.23 \pm 6.75\%$ was observed at 2 h compared to $47.78 \pm 7.74\%$ in pre-exposed control mice. CNR attenuation decreased with time to become comparable to control value at 1-week investigation time point. In sub-acute treatment group, CNR attenuation of $85.76 \pm 6.11\%$ was observed at 24 h and decreased gradually with time to become statistically equivalent to control values starting from 2-weeks investigation time points.

On the other hand, no signs of any inflammatory reactions were observed in the lungs following intrapulmonary administration of the different SPIONs formulations in both acute and sub-acute treatments groups with no detection of hyper-intensity regions related to edema secretion in lung MR images.

Abdominal MRI which was performed to assess the possibility of SPIONs translocation to systemic abdominal organs after their intrapulmonary administration did not revealed any MR signal intensity variation in the organs of interest (i.e. liver, spleen and kidneys) following single dose administration of the different SPIONs formulations in acute treatment groups (Figure 2). Interestingly, a statistically significant attenuation in CNR was only detected in the liver at 24 h investigation time point after intrapulmonary administration of three consecutive doses of SPIONs in sub-acute treatment groups. No other anatomical alterations were visually observed in mice body organs during the 1-month follow-up investigation.

Iron quantification using ICP-MS

Iron concentrations quantified using ICP-MS in the lung confirmed the deposition of SPIONs in the lung following their intrapulmonary administration using the MicroSprayer aerosolizer. Quantitatively, following administration of a single dose of SPIONs (i.e. 0.8 mmol of iron kg^{-1} corresponding to 0.1 mg of iron per mice), 0.345 mg Fe/g increase in iron content was measured in the lung at 2 h post-administration in the SPION group (i.e. approximately 70% of administered dose) compared to control mice. Iron content decreased gradually with time in the lung to become comparable to control values at 1-week investigation time point (Figure 3a). Following three consecutive administrations of SPIONs with 24 h intervals (i.e. total doses = 0.3 mg), 0.715 mg Fe/g increase in iron content was quantified in the lung at 24 post last administration (i.e. approximately 50% of the three administered doses) compared to control mice. As expected, iron content also regressed in a time-dependent manner to become non-statistically different from control mice at 1-month investigation time points. A similar profile was observed for the different SPIONs formulations (i.e. PEG functionalization with either carboxyl or amine modification).

While no increase was measured in both spleen and kidneys for all groups, interestingly, a statistically significant increase was observed in the liver at 24 h following three doses administration in sub-acute set, confirming the noninvasive MRI readouts (Figure 3b–d). Quantitatively, an increase of 0.048 mg Fe/g was detected in the liver of SPION group (i.e. approximately 14%) compared to control mice.

Oxidative stress evaluation (TBARS assay)

Biocompatibility evaluation was first performed using TBARS assay to evaluate the overall oxidative stress induced by the different SPIONs formulations in both acute and sub-acute sets. Following acute exposure, a significant ($p < 0.05$) increase in lipid peroxidation was evident in BALF and lung samples until 1 week with a more prominent effect observed in lung biopsy samples (Figure 4). A similar profile was observed in sub-acute treatment set. The increase in lipid peroxidation gradually regressed in a time-dependent manner to become comparable to control values at 1-month investigation time point.

Quantitatively, in both acute and sub-acute animal sub-sets, the relative oxidative stress was found to be significantly lower after PEG surface functionalization with no substantial difference observed between carboxyl and amine terminal modifications.

DNA damage assessment (comet assay)

To investigate the effect of SPIONs with their further surface modification at the level of DNA, a single-cell gel electrophoresis (i.e. comet assay) in alkaline conditions was performed to visualize DNA fragments microscopically on cells from BALF and lung biopsy samples. An increase in DNA damage was observed after single and to a higher extent three consecutive

RIGHTSLINK

Nanotoxicology Downloaded from informahealthcare.com by 212.215.215.114 on 11/19/14
For personal use only.

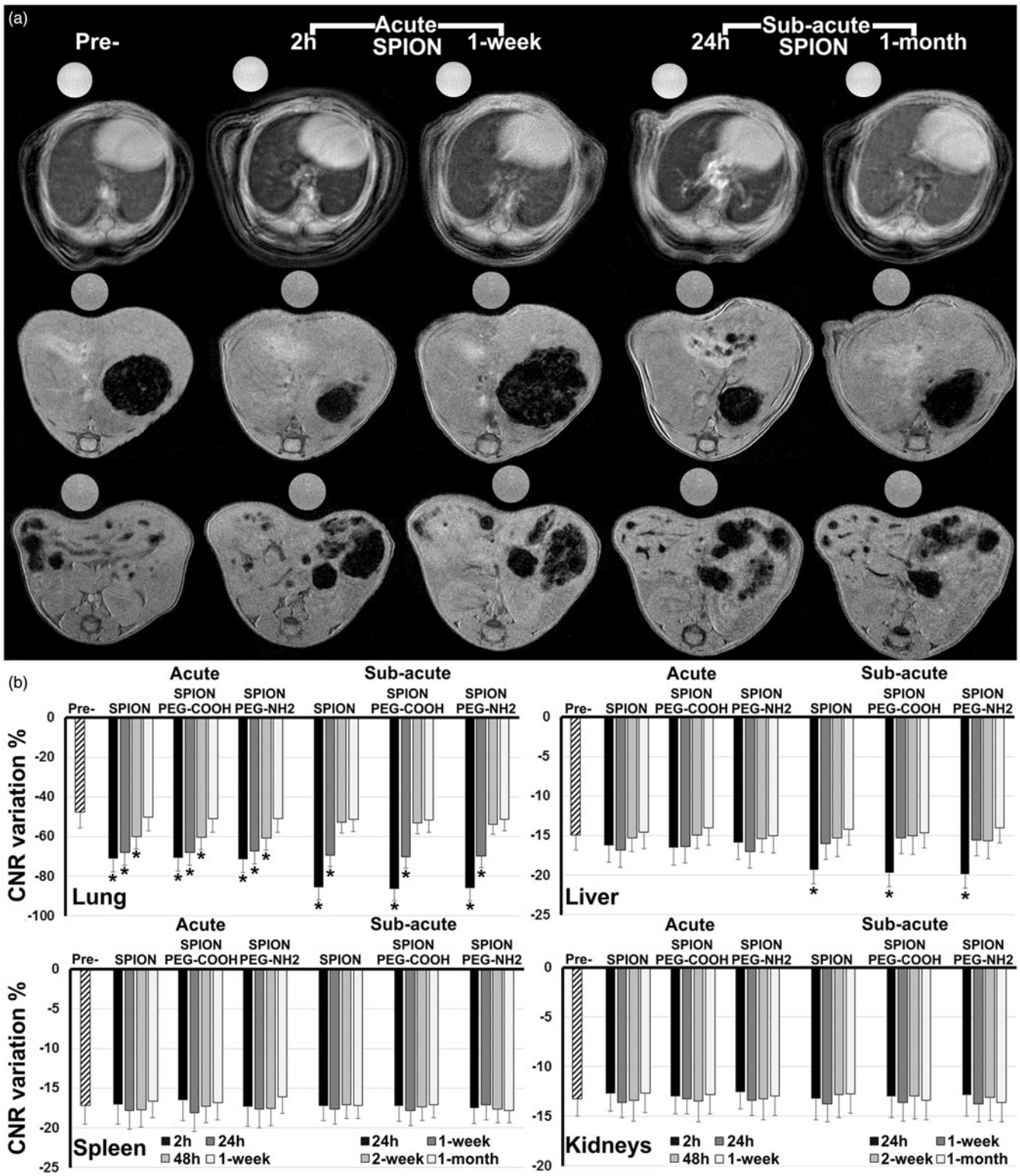

Figure 2. (a) Representative MR images of lung (upper row), liver (middle row) and spleen and kidneys (lower row) in mice pre- and post-intrapulmonary administration of SPION at 2 h and 1 week in acute set and 24 h and 1 month in sub-acute set. (b) Percentage of CNR variation in the lung, liver, spleen and kidneys in mice pre- and post-intrapulmonary administration of SPION before and after their surface functionalization with either PEG-COOH or PEG-NH2 at the different investigation time points in acute and sub-acute sets. Data expressed as mean ± standard deviation, $n = 6$ per group. $^*p < 0.05$.

doses administration of nanoparticles until 1-week exposure time (Figure 5). The extent of DNA damage was notably greater with SPIONs compared to either PEG-COOH or PEG-NH_2 functionalized nanoparticles. A slightly more prominent DNA damage was more observed with negatively charged compared to positively charged nanoparticles at the different investigation time points. By the completion of 1 week, a considerable decrease in the extent of DNA damage was observed in all treatments for both single and multiple doses of nanoparticles in BALF as well as lungs biopsies samples. However, by the completion of the

RIGHTSLINK

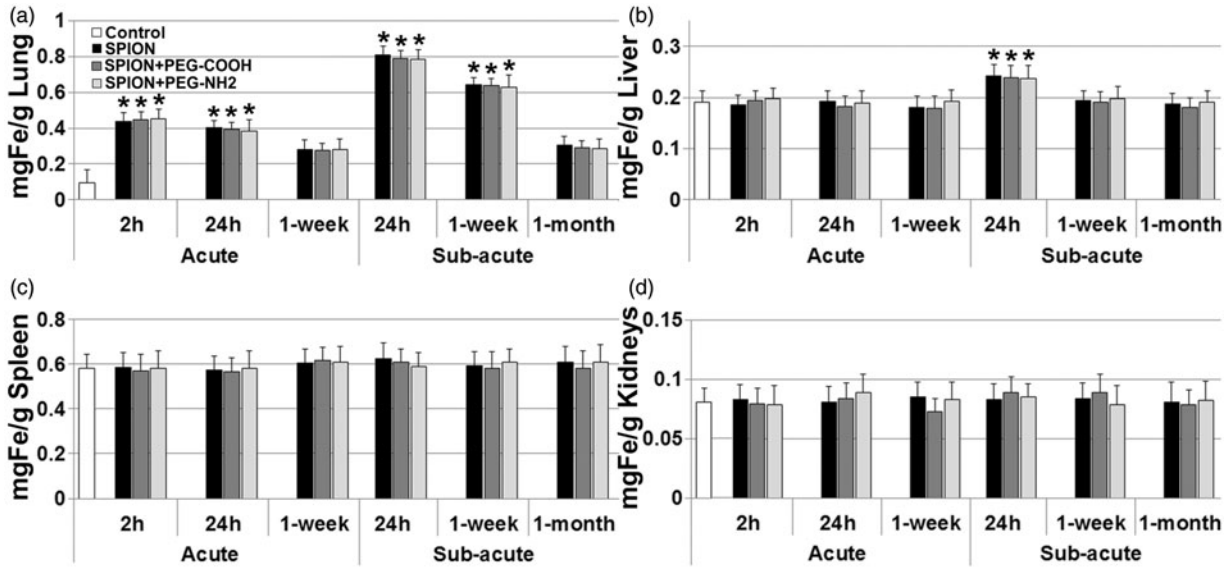

Figure 3. Iron content in mg Fe/g of organ sample quantified using ICP-MS in the lung (a), liver (b), spleen (c) and kidneys (d) following intrapulmonary instillation of SPION before and after their surface functionalization with either PEG-COOH or PEG-NH_2 at different investigation time points in acute and sub-acute sets. Data expressed as mean ± standard deviation, $n = 3$ per group. *$p < 0.05$.

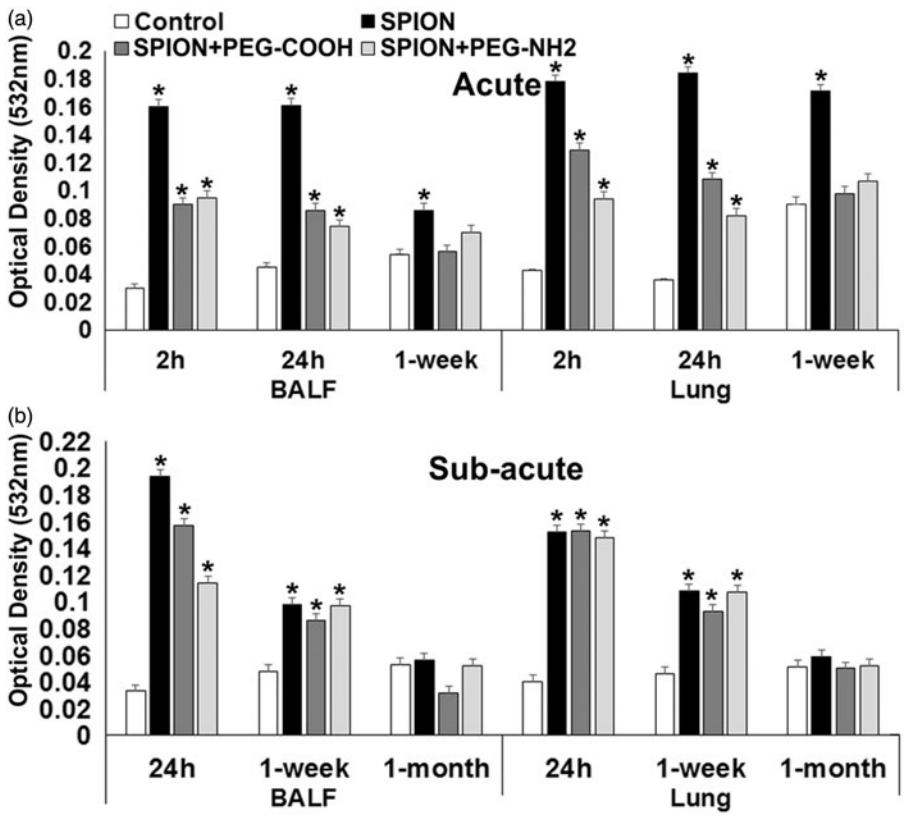

Figure 4. Lipid peroxidation (TBARS assay) assessed on BALF or lung biopsy samples to evaluate the overall oxidative stress induced by intrapulmonary exposition of SPION before and after their surface functionalization with either PEG-COOH or PEG-NH_2 at different investigation time points in (a) acute and (b) sub-acute sets. Optical density of the samples was measured at 532 nm. Data expressed as mean ± standard deviation, $n = 3$ per group. *$p < 0.05$.

1-month follow-up study, the level of DNA damage became comparable to control values for the different SPION formulations.

Gene expression profile (real-time polymerase chain reaction)

To further evaluate the biological effect of intrapulmonary administration of SPIONs before and after their PEG surface modification, the relative gene expression in selected mediators such as NOS-2, CXCL-10, CCL-17, CCL-22 and IL-10 was analyzed on lung biopsies using RT-PCR and compared with control mice. Following a single-dose lung administration of SPION in acute set, a considerable increase in CCL-17 and IL-10 expression markers was observed within 2 h post-exposure, with a maximum of 4.15-fold increase relative to control mice for IL-10 (Figure 6a). Comparing the three SPIONs formulations, and as expected, SPION without further surface modification with PEG caused a prominent increase in the tested markers. SPION functionalized with PEG-COOH was shown to induce a slightly

Nanotoxicology Downloaded from informahealthcare.com by 212.215.215.114 on 11/19/14
For personal use only.

RIGHTSLINK

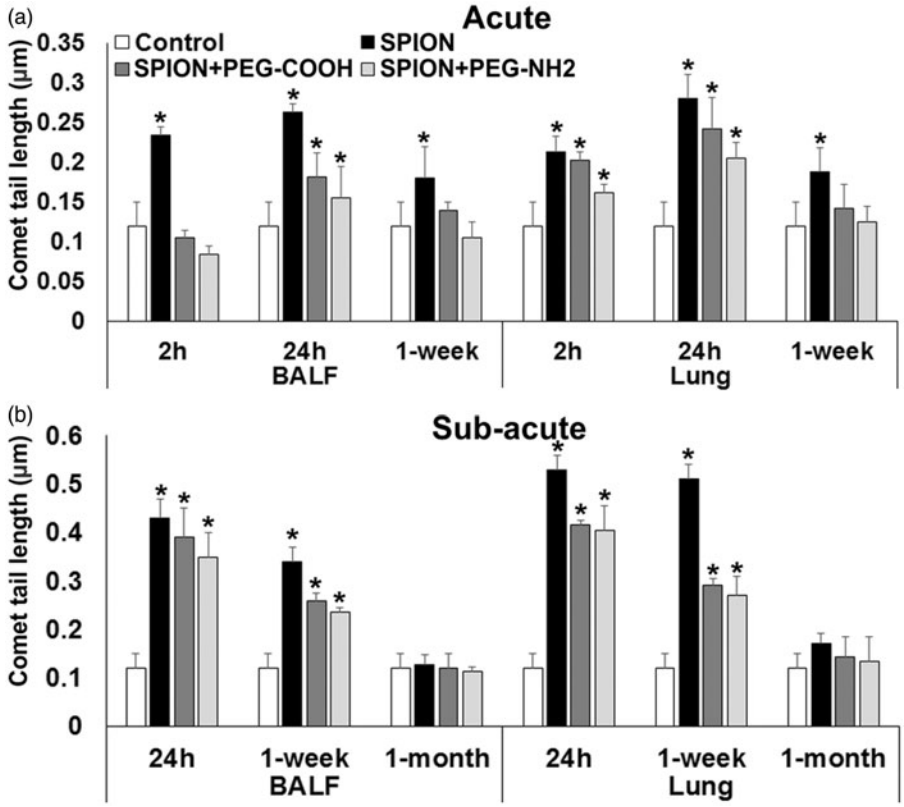

Figure 5. Comet tail length assessed on cells from BALF or lung biopsy samples as an effective method to evaluate the possible DNA damage induced by intrapulmonary exposition of SPION before and after their surface functionalization with either PEG-COOH or PEG-NH_2 at different investigation time points in (a) acute and (b) sub-acute sets. Optical density of the samples was measured at 532 nm. Data expressed as mean ± standard deviation for an average of 100 cells, $n = 3$ per group. $*p < 0.05$ versus control.

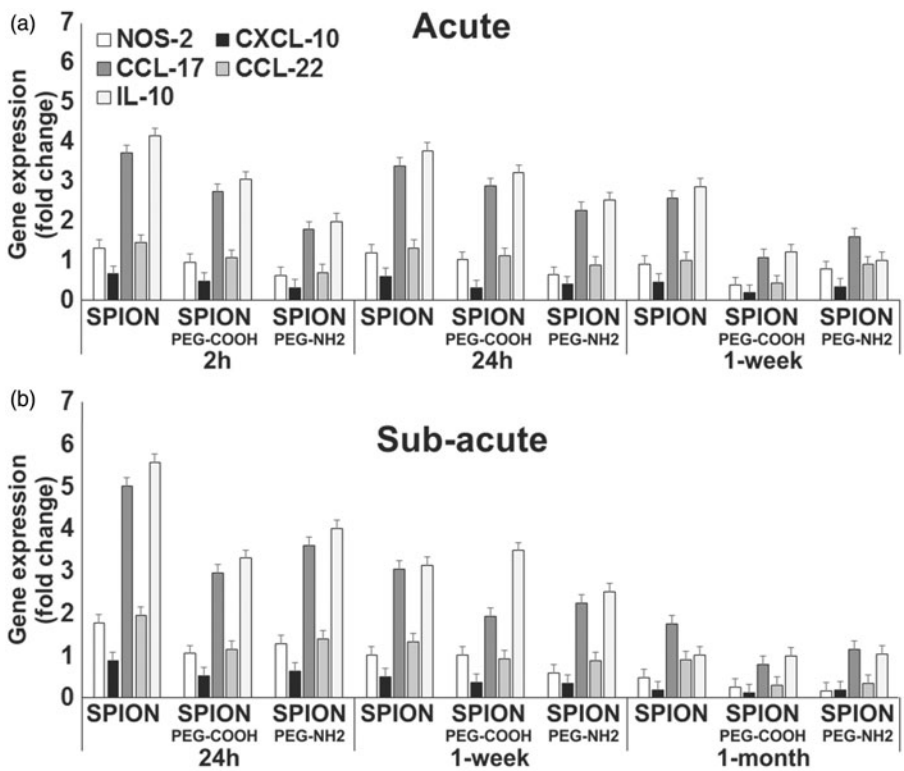

Figure 6. Relative gene expression (fold change) of NOS-2, CXCL-10, CCL-17, CCL-22 and IL-10 in lung biopsies of mice following their intrapulmonary exposition with SPIONs before and after their surface functionalization with either PEG-COOH or PEG-NH_2 at different investigation time points in (a) acute and (b) sub-acute sets, compared with control mice. Data expressed as mean ± standard deviation, $n = 3$ per group.

more increase in gene expression compared to PEG-NH_2 functionalization. Interestingly, 1-week post-administration, the expression of almost all gene markers decreased and became comparable to control values for both PEGylated groups. Following exposure of mice with three consecutive doses of nanoparticles (i.e. sub-acute set), a similar trend was observed with elevations in all tested gene markers compared to control group at 24 h and 1-week investigation time points (Figure 6b). However, a substantial decrease in all gene markers was observed at 1-month investigation time point.

Nanotoxicology Downloaded from informahealthcare.com by 212.215.215.114 on 11/19/14
For personal use only.

RIGHTSLINK

Discussion

A wide range of factors including size, coating, surface charge, physicochemical properties, etc., have been shown to influence the biocompatibility of superparamagnetic iron oxide nanoparticles (Ai et al., 2011). The surface charge coating of SPION largely determines the cell-to-cell interactions in both *in vitro* and *in vivo* test systems. Therefore, for their safe prospective clinical applications as therapeutic and diagnostic nanocarriers for pulmonary diseases, SPION biocompatibility must be evaluated (Warheit & Donner, 2010). This study was therefore conducted to understand the biological impact of SPION functionalization with polyethylene glycol having either negative or positive surface charge, following their intrapulmonary administration in a mouse model. Noninvasive free-breathing MR imaging protocols were first performed to validate SPIONs detection in the lung using ultra-short echo time sequence and their possible subsequent translocation to abdominal organs using susceptibility-weighted gradient echo sequence. Iron quantification using ICP-MS was then performed to confirm MRI readouts. Oxidative stress induction, cellular DNA damage and relative gene expression of several biomarkers of interest have been conducted to assess the biocompatibility of SPIONs following either acute or sub-acute intrapulmonary administration in a 1-month follow-up study.

With their high magnetization effect and specific power absorption rate (Grüttner et al., 2007), nanoferrite SPIONs were preferred in this study for their promising prospective applications in magnetic hyperthermia and magnetic targeting (Hilger & Kaiser, 2012) as theranostics nanoprobes for the treatment of pulmonary diseases. These SPIONs showed a very high $r2^*$ transverse relaxivitiy value compared to the reported values for clinically approved MRI contrast agents such as Feridex® IV (Berlex Laboratories, Wayne, NJ) or Resovist® (Bayer Healthcare, Berlin, Germany) at the same magnetic field (Rohrer et al., 2005), which improved their sensitive detection especially in the lung with limited MRI signal. Among various surface coating materials previously proposed, dextran-coated SPIONs have shown enhanced biocompatibility (Luengo et al., 2013) and were therefore preferred in this study to investigate the effect of their further PEG modification with either negatively or positively charged terminals.

It has been reported that the surface charge of iron oxide nanoparticles should ideally be maintained at neutral or close to neutral for imaging and drug delivery (Prodan et al., 2014). Therefore, slight positively or negatively charged SPIONs were preferred. $COOH^-$ and NH_2^- terminals offer the possibility for their prospect coupling with antibodies or other bioactive agents using different conjugation techniques.

Pulmonary MR imaging was limited because of the difficulties to image the lung due to factors such as signal loss due to cardiac pulsation and respiration, susceptibility artifacts caused by multiple air–tissue interfaces and low proton density. However, since the introduction of UTE sequence (Tyler et al., 2007), we have successfully applied it to sensitively detect free SPIONs or iron-loaded cells in the lung (Al Faraj et al., 2012, 2014a,b).

Following exposure of the different SPION formulations, no difference in MR signal attenuation was observed. This signal attenuation regressed in a time-dependent manner due to their elimination by the mucus or their degradation by alveolar macrophages. On the other hand, MR acquisitions using UTE sequence which was validated to allow better detection of inflammatory regions in the lung (i.e. hyper-intensity related to edema secretion), sometimes undetectable using standard gradient echo sequences (Conti et al., 2010), did not reveal any sign of inflammatory reactions following SPION exposure in both acute and sub-acute treatment groups.

While some studies have reported the translocation of nanoparticles such as ferric oxide, gold and titanium dioxide following their lung administration, other reports examining various materials like iron oxide, titanium dioxide, silica and copper nanoparticles, suggested that they are not capable of passing from the lung to the systemic abdominal organs via the circulatory system (Prodan et al., 2014).

In our study, abdominal MRI performed to assess the possibility of SPIONs translocation to systemic abdominal organs revealed a statistically significant transient accumulation in the liver following high-dose administration (i.e. three consecutive doses of 0.1 mg of iron at 24 h intervals in sub-acute treatment groups) while no translocation was observed following single-dose exposure. Similar biodistribution was perceived for different SPION formulations. These observations were confirmed by ICP-MS iron quantification.

It has been reported (Zhu et al., 2008) that following their intrapulmonary administration, the nanoparticles capable of entering into blood circulation will first accumulate in the liver as the major organ for biotransformation of toxins. Although, this study provided preliminary evidence of possible translocation of high dose of SPIONs to the liver after their lung administration, further confirmatory studies are required to conclusively establish this observation and investigate the various physicochemical properties allowing this phenomenon (i.e. size, composition, dose, exposure technique, coating materials).

On the other hand, although it has been widely considered that SPIONs have relatively low or no cytotoxicity compared to other nanoparticle formulations, it must be emphasized that minor levels of oxidative stress can cause disruption of cell function by causing subtle but deleterious levels of DNA damage (Singh et al., 2010). Therefore, a combination of oxidative stress assessment, DNA damage analysis at cellular level and relative gene expression of several biomarkers have been performed in the present study. While the different formulations of SPIONs caused a significant increase in oxidative stress following both acute and sub-acute exposure, as expected, the levels of lipid peroxidation progressively returned to normal in both BALF and lungs. Overall, the levels of oxidative stress were found significantly higher for non-PEGylated SPIONs compared to both positively- and negatively-charged PEGylated nanoparticles, which showed comparable values.

Although we believe that the exposure procedure might affect this increase in oxidative stress at short investigation time point, the link between SPION-induced oxidative stress and the cell toxicity is thought either due to the generation of reactive metabolites or through peroxidase-like activity (Zhuang et al., 2012). While PEG functionalization was reported to improve the biocompatibility of nanoparticles, the effect of their surface charge is still not conclusive. While some studies reported that positively charged SPIONs were more internalized with consequent higher toxicity (Cengelli et al., 2006), other studies showed that the negatively charged nanoparticles showed uptake and toxicity subject to their coating (Villanueva et al., 2009) and their internalization may occur through nonspecific binding and clustering on cationic sites on the cell membrane (Verma & Stellacci, 2010).

To further investigate the effects of SPIONs and their further surface modification with PEG-COOH or PEG-NH_2 on the ability to cause genetic alterations, the extent of DNA damage for individual cells was assessed. PEGylated SPIONs with either negative or positive surface charge showed much lower increase of DNA damage compared to non-PEGylated SPIONs. In contrast to oxidative stress assessment, that showed similar levels for both surface functionalization, the DNA damage was slightly higher with negatively charged compared to positively charged

Nanotoxicology Downloaded from informahealthcare.com by 212.215.215.114 on 11/19/14
For personal use only.

RIGHTSLINK

nanoparticles at the different investigation time points. However, post 1-week, all animals showed minimal DNA damage with levels similar to controls possibly indicative of the ability of host cells to repair the DNA using the DNA repair mechanisms. The precise mechanisms that cause genotoxic effects of nanoparticles are still not conclusive, although size and surface charge are known to potentially affect DNA damage. The results from this study may indicate that surface charge may have induced the DNA damage; however, additional studies with more exposure time points are needed for conclusive results.

In addition to the above experiments, an evaluation of the effect of SPIONs on the relative gene expression of several cell mediators such as NOS-2, CXCL-10, CCL-17, CCL-22 and IL-10 was analyzed in the lung of mice. A notable increase in gene expression of CCL-17 and IL-10 was observed in SPIONs followed by SPION + PEG-COOH and to a lower extent in SPION + PEG-NH_2. However, all expression profiles regressed in a time-dependent manner to normal values.

Evaluation of the effect of nanoparticles at the level of gene, which help specifying the alterations in expression profiles of cell mediators, can play an important role in understanding the effect of nanoparticles on cell signaling and/or inflammatory pathways (Sood et al., 2011). Local adverse reactions induced by the nanoparticles could have caused elevations in CCL-17 and IL-10 along with other mediators as biomarkers of immunotoxicity to help regulating the immune system function (Elsabahy & Wooley, 2013).

While this increase might indicate the role of administrated nanoparticles at the level of gene expression, it should be emphasized that such an increase may be attributed to the capacity of host system to successfully tackle their genotoxicity and is of particular importance for clinical developments of theranostic nanocarriers. This aspect, however, needs further evaluation to precisely understand their potential implications at the cellular and molecular levels.

Conclusion

In conclusion, pulmonary MR imaging using UTE sequence allowed successful sensitive detection of SPIONs in the lung. While the possibility of SPION passage through the alveolar–capillary barrier is still not conclusive, our results showed a transient translocation of SPIONs in the liver following three consecutive intrapulmonary administration of 0.1 mg per mouse, noninvasively detected using MRI and confirmed using ICP-MS. However, further confirmatory studies are required to conclusively establish this observation and investigate the various physicochemical properties allowing this phenomenon (i.e. size, composition, dose, exposure technique, coating materials).

Oxidative stress induction and genotoxicity assessments (i.e. DNA damage and relative gene expression) demonstrated that surface charge modification with polyethylene glycol remarkably improved the biocompatibility of SPIONs after their intrapulmonary administration in a murine model in both acute and subacute sets, with no significant difference observed between negative and positive terminal modifications.

These observations open novel perspective for safe application of polyethylene glycol functionalized dextran-coated iron oxide nanocarriers functionalized with either carboxyl or amine terminals, offering the possibility for their prospect coupling with antibodies or other bioactive agents as novel theranostic nanoprobes for the treatment of several pulmonary diseases.

Acknowledgements

We thank Saud Alotaibi for general help in this work, Dr. Cordula Gruettner from Micromod Partikeltechnologie GmbH for SPION design and characterization and Dr. G. Holzhueter from the University of Rostock for the TEM imaging.

Declaration of interest

This work was supported by National Science Technology and Innovation plan NSTIP strategic technologies programs, project number 12-MED2536, in the Kingdom of Saudi Arabia.

References

Ai J, Biazar E, Jafarpour M, Montazeri M, Majdi A, Aminifard S, et al. 2011. Nanotoxicology and nanoparticle safety in biomedical designs. Int J Nanomedicine 6:1117–27.

Al Faraj A, Gazeau F, Wilhelm C, Devue C, Guerin CL, Pechoux C, et al. 2012. Endothelial cell-derived microparticles loaded with iron oxide nanoparticles: feasibility of MR imaging monitoring in mice. Radiology 263:169–78.

Al Faraj A, Shaik AS, Afzal S, Al Sayed B, Halwani R. 2014a. MR imaging and targeting of a specific alveolar macrophage subpopulation in LPS-induced COPD animal model using antibody-conjugated magnetic nanoparticles. Int J Nanomed 9:1491–503.

Al Faraj A, Sultana Shaik A, Pureza MA, Alnafea M, Halwani R. 2014b. Preferential macrophage recruitment and polarization in LPS-induced animal model for COPD: noninvasive tracking using MRI. PLoS One 9:e90829.

Azarmi S, Roa WH, Lobenberg R. 2008. Targeted delivery of nanoparticles for the treatment of lung diseases. Adv Drug Deliv Rev 60:863–75.

Bailey MM, Berkland CJ. 2009. Nanoparticle formulations in pulmonary drug delivery. Med Res Rev 29:196–212.

Bernd H, De Kerviler E, Gaillard S, Bonnemain B. 2009. Safety and tolerability of ultrasmall superparamagnetic iron oxide contrast agent: comprehensive analysis of a clinical development program. Invest Radiol 44:336–42.

Braakhuis H, Park M, Gosens I, De Jong W, Cassee F. 2014. Physicochemical characteristics of nanomaterials that affect pulmonary inflammation. Part Fibre Toxicol 11:18.

Cengelli F, Maysinger D, Tschudi-monnet F, Montet X, Corot C, Petri-Fink A, et al. 2006. Interaction of functionalized superparamagnetic iron oxide nanoparticles with brain structures. J Pharmacol Exp Ther 318:108–16.

Chellat F, Merhi Y, Moreau A, Yahia L. 2005. Therapeutic potential of nanoparticulate systems for macrophage targeting. Biomaterials 26: 7260–75.

Conti G, Tambalo S, Villetti G, Catinella S, Carnini C, Bassani F, et al. 2010. Evaluation of lung inflammation induced by intratracheal administration of LPS in mice: comparison between MRI and histology. Magn Reson Mater Phys Biol Med 23:93–101.

Corot C, Robert P, Idee JM, Port M. 2006. Recent advances in iron oxide nanocrystal technology for medical imaging. Adv Drug Deliv Rev 58: 1471–504.

Elsabahy M, Wooley KL. 2013. Cytokines as biomarkers of nanoparticle immunotoxicity. Chem Soc Rev 42:5552–76.

Frohlich E. 2012. The role of surface charge in cellular uptake and cytotoxicity of medical nanoparticles. Int J Nanomed 7:5577–91.

Geiser M, Kreyling WG. 2010. Deposition and biokinetics of inhaled nanoparticles. Part Fibre Toxicol 7:2.

Grüttner C, Müller K, Teller J, Westphal F, Foreman A, Ivkov R. 2007. Synthesis and antibody conjugation of magnetic nanoparticles with improved specific power absorption rates for alternating magnetic field cancer therapy. J Magn Magn Mater 311:181–6.

Hamman JH, Enslin GM, Kotze AF. 2005. Oral delivery of peptide drugs: barriers and developments. BioDrugs 19:165–77.

Hilger I, Kaiser WA. 2012. Iron oxide-based nanostructures for MRI and magnetic hyperthermia. Nanomedicine (Lond) 7:1443–59.

Luengo Y, Nardecchia S, Morales MP, Serrano MC. 2013. Different cell responses induced by exposure to maghemite nanoparticles. Nanoscale 5:11428–37.

Mbeh DA, Franca R, Merhi Y, Zhang XF, Veres T, Sacher E, et al. 2012. In vitro biocompatibility assessment of functionalized magnetite nanoparticles: biological and cytotoxicological effects. J Biomed Mater Res A 100:1637–46.

Nanotoxicology Downloaded from informahealthcare.com by 212.215.215.114 on 11/19/14
For personal use only.

RIGHTSLINK

Prodan AM, Ciobanu CS, Popa CL, Iconaru SL, Predoi D. 2014. Toxicity evaluation following intratracheal instillation of iron oxide in a silica matrix in rats. BioMed Res Int 2014:Article ID 134260, 13 pages.

Rohrer M, Bauer H, Mintorovitch J, Requardt M, Weinmann HJ. 2005. Comparison of magnetic properties of MRI contrast media solutions at different magnetic field strengths. Invest Radiol 40:715–24.

Rosen JE, Chan L, Shieh DB, Gu FX. 2012. Iron oxide nanoparticles for targeted cancer imaging and diagnostics. Nanomedicine 8:275–90.

Singh N, Jenkins GJ, Asadi R, Doak SH. 2010. Potential toxicity of superparamagnetic iron oxide nanoparticles (SPION). Nano Rev 1. doi: 10.3402/nano.v1i0.5358.

Singh N, Jenkins GJ, Nelson BC, Marquis BJ, Maffeis TG, Brown AP, et al. 2012. The role of iron redox state in the genotoxicity of ultrafine superparamagnetic iron oxide nanoparticles. Biomaterials 33:163–70.

Sood A, Salih S, Roh D, Lacharme-Lora L, Parry M, Hardiman B, et al. 2011. Signalling of DNA damage and cytokines across cell barriers exposed to nanoparticles depends on barrier thickness. Nat Nanotechnol 6:824–33.

Sung JC, Pulliam BL, Edwards DA. 2007. Nanoparticles for drug delivery to the lungs. Trends Biotechnol 25:563–70.

Tyler DJ, Robson MD, Henkelman RM, Young IR, Bydder GM, et al. 2007. Magnetic resonance imaging with ultrashort TE (UTE) PULSE sequences: technical considerations. J Magn Reson Imaging 25: 279–89.

van Rijt SH, Bein T, Meiners S. 2014. Medical nanoparticles for next generation drug delivery to the lungs. Eur Respir J 44:765–74.

Verma A, Stellacci F. 2010. Effect of surface properties on nanoparticle–cell interactions. Small 6:12–21.

Villanueva A, Canete M, Roca AG, Calero M, Veintemillas-Verdaguer S, Serna CJ, et al. 2009. The influence of surface functionalization on the enhanced internalization of magnetic nanoparticles in cancer cells. Nanotechnology 20:115103.

Wahajuddin, Arora S. 2012. Superparamagnetic iron oxide nanoparticles: magnetic nanoplatforms as drug carriers. Int J Nanomed 7:3445–71.

Warheit DB, Donner EM. 2010. Rationale of genotoxicity testing of nanomaterials: regulatory requirements and appropriateness of available OECD test guidelines. Nanotoxicology 4:409–13.

Xu C, Sun S. 2013. New forms of superparamagnetic nanoparticles for biomedical applications. Adv Drug Deliv Rev 65:732–43.

Yoo D, Lee JH, Shin TH, Cheon J. 2011. Theranostic magnetic nanoparticles. Acc Chem Res 44:863–74.

Zhu MT, Feng WY, Wang B, Wang TC, Gu YQ, Wang M, et al. 2008. Comparative study of pulmonary responses to nano- and submicron-sized ferric oxide in rats. Toxicology 247:102–11.

Zhuang J, Fan K, Gao L, Lu D, Feng J, Yang D, et al. 2012. Ex vivo detection of iron oxide magnetic nanoparticles in mice using their intrinsic peroxidase-mimicking activity. Mol Pharm 9:1983–9.

Supplementary material available online

Nanotoxicology Downloaded from informahealthcare.com by 212.215.215.114 on 11/19/14
For personal use only.

RIGHTSLINK

View publication stats